Soft Matter

PAPER

View Article Online
View Journal

Cite this: DOI: 10.1039/c6sm02239a

Morphology dictated heterogeneous dynamics in two-dimensional aggregates

Tamoghna Das,†[a] T. Lookman[b] and M. M. Bandi*[c]

Received 2nd October 2016,
Accepted 7th November 2016

DOI: 10.1039/c6sm02239a

www.rsc.org/softmatter

Particulate aggregates occur in a variety of non-equilibrium steady-state morphologies ranging from finite-size compact crystalline structures to non-compact string-like conformations. This diversity is due to the competition between pair-wise short range attraction and long range repulsion between particles. We identify different microscopic mechanisms in action by following the simulated particle trajectories for different morphologies in two dimensions at a fixed density and temperature. In particular, we show that the compact clusters are governed by symmetric caging of particles by their nearest neighbors while sidewise asymmetric binding of particles leads to non-compact aggregates. The measured timescales for these two mechanisms are found to be distinctly different providing phenomenological evidence of a relation between microstructure and dynamics of particulate aggregates. Supporting these findings, the time dependent diffusivity is observed to differ across the morphological hierarchy, while the average long-time dynamics is, in general, sub-diffusive at 'low' temperatures. Finally, one generic relation between diffusivity and structural randomness, applicable to simple equilibrium systems, is validated for complex aggregate forming systems through further analysis of the same system at different temperatures.

1 Introduction

Relating the morphology and dynamics of non-equilibrium systems has remained a challenge despite concerted theoretical and experimental efforts[1–4] over the years. Systems driven out of equilibrium, such as glassy and granular materials, exhibit dynamic structural order,[5,6] which often extends over multiple length and time scales without any clear separation between them. The effect of geometry on dynamics[7,8] is also expected in systems confined by external fields or porous media. Transport within crowded environments such as living cells[9] presents yet another example where spatial structure and dynamics show strong co-dependence. Yet another emergent and active field of research focuses on artificially assembled superstructures of particles[10–16] at nanoscale and mesoscale, by taking advantage of recent advances in chemical synthesis and experimental techniques. Such fabricated assembly of particles provides an elegant model system to understand the complex interplay between microstructure and microscopic dynamics of real systems for several reasons. The degree of (dis-)order in such systems can be easily tuned *in situ* and simultaneous precise quantifications are possible *via* standard experimental techniques such as electron microscopy and X-ray scattering. Further, the possibility of achieving a targeted response from a specific superstructure promises the essential technological incentives to study these particulate assemblies thoroughly.

Here, we present a detailed simulation study of both global and local dynamics of a generic non-equilibrium pattern forming particulate system, namely, two-dimensional (2D) aggregates. By following the steady state trajectories simulated by molecular dynamics, we provide phenomenological evidence of direct correspondence between the microscopic dynamics and structural hierarchy in 2D aggregates. Particulate aggregates may occur in a broad range of structural randomness (or order)[17–24] between liquids and crystalline solids due to the competition between pair-wise short range attraction and long range repulsion. The presence of multiple length scales due to competing interactions introduces geometric frustration at the interaction level and complex structural, thermodynamic and dynamic behavior are expected as a result. Such systems were introduced[25] as a natural extension of van der Waals theory of simple liquids with a single length and time scale. The unusual thermodynamics originating from multi-length scale physics has also been extensively explored[26,27] theoretically. However, any experimental realization of such a system has had to wait for sophisticated chemical processing of colloidal and nanoparticle systems until very recently.

In general, the aggregates are experimentally formed by quenching a high-temperature equilibrium liquid[28,29] to a

[a] Collective Interactions Unit, OIST Graduate University, Onna, Okinawa 9040495, Japan. E-mail: tamoghna.das@nist.gov
[b] Theoretical Division, Los Alamos National Laboratory, Los Alamos, NM 87545, USA. E-mail: txl@lanl.gov
[c] Collective Interactions Unit, OIST Graduate University, Onna, Okinawa 9040495, Japan. E-mail: bandi@oist.jp
† Present address: University of Maryland, College Park, MD 20742 and National Institute of Standards and Technology, Gaithersburg, MD 20899, USA.

much lower temperature. While such a dynamical preparation protocol is useful in practice, it invariably drives the system out of equilibrium. The inherent geometric frustration together with the non-equilibrium dynamics, then, pose serious difficulties for unambiguous identification of the key elements behind the resulting rich phenomenology. Different mechanisms such as diffusion-limited[30] and reaction-limited aggregation[31] have been reported. Stemming from a fast quench, the glass transition scenario has been conjectured[32,33] and quite thoroughly investigated. To describe the phase behavior of such systems, both equilibrium routes[34,35] and kinetic viewpoint,[36–38] have also been explored quite extensively. However, a conclusive theoretical understanding of the process is yet to be achieved.[39–43] To focus on the effect of geometric frustration alone, a 'slow' cooling protocol is adapted, in the present study, to achieve aggregate formation in contrast to the usual quench from high temperature. Upon reaching the desired value, the final temperature is maintained constant over a long observation time. The steady state dynamics are non-equilibrium, sub-diffusive and heterogeneous for all aggregate morphologies. While phase separation seems to affect the overall dynamics of the system, local slow dynamics results from the reduced thermal fluctuations at final 'low' temperatures. Individual particle trajectories and their spatio-temporal correlations reveal that systems with different morphologies under same thermodynamic conditions evolve *via* different microscopic dynamics. One distinct change in the microscopic time scales across the morphological hierarchy of aggregates is identified and a scaling relation between the average dynamics and structural randomness of the system is demonstrated.

The organization of the paper is as follows: to set up the background for this study, we provide the essential information in Section 2 in three parts, (i) the specific form and tuning parameters of competing interactions, (ii) the details of molecular dynamics simulation and cooling protocol used to prepare the model system and (iii) a brief description of the morphological variations obtained by tuning the interactions. In Section 3, we elaborate the main results on dynamics in two parts, (i) comparison of particle dynamics at a fixed low temperature for different morphologies and (ii) global dynamics and its temperature dependence. The results are summarized and further implications are discussed in Section 4.

2 Model, methods and morphology

The model system with competing interactions

Competing interactions are necessary for aggregate formation[44] and can occur in diverse physical settings,[45–48] each having its own set of control parameters.[49] Our choice of model system is a reliable representation of globular proteins,[50] engineered colloids[51] and nanoparticles.[52] In this model, the short-range attraction and long-range repulsion are realized by a generalized Lennard-Jones potential and a pair-wise potential of Yukawa form, respectively,

$$\phi_{SA} = 4\varepsilon[(\sigma/r)^{2\alpha} - (\sigma/r)^{\alpha}] \quad (1)$$

$$\phi_{LR} = (A\sigma/r)\exp(-r/\xi) \quad (2)$$

The length and energy scales are set by σ and ε respectively. The range of attraction realized by the well-width of the bare $2\alpha - \alpha$ potential is controlled by α. This range is 0.2σ for our choice α = 18 while it extends to 2.5σ for the usual Lennard-Jones potential with α = 6. We note that the thermodynamic properties of a particulate system with bare attraction[53] are independent of α for $\alpha \geq 18$. The Yukawa part implicitly models the long-range repulsive effect of surrounding weakly polar media. The strength of repulsion A and the screening length ξ are measured in ε and σ units respectively. The implicit solvent description is particularly relevant for the polymer grafted nanoparticle systems[54] where the sparse monomers act as an effective medium in the absence of a real one. The effective centro-symmetric interaction, $\phi = \phi_{SA} + \phi_{LR}$, has a positive energy barrier at finite distance, which is separated from the steep hard core repulsion by an attractive minimum (Fig. 1). The height and extent of the barrier can be controlled by A and ξ. For the present study, we limit ourselves over a restricted parameter space to focus on the dynamics. Specifically, we fix the value of repulsion strength, A, throughout the study, to 4 (in ε units) to match the strength of attraction exactly. The range of repulsion set by the screening length, ξ is varied from 0.5 to 0.8 (in σ units). Note that the global attractive minimum of the effective pair-potential ϕ becomes local and positive as ξ is increased from 0.5 to 0.8 (Fig. 1). The low temperature local dynamics of the system is compared only for these two limiting cases which produce distinctly different morphology. The change in morphology is briefly described separately at the end of this section. Temperature dependence of the global dynamics is presented for the whole range of ξ.

Simulation details and cooling protocol

We consider a 2D system of interacting mono-disperse particles at fixed density ρ = 0.4. The initial configuration is a random non-overlapping arrangement of N = 56 000 particles of unit mass in a $376\sigma \times 372\sigma$ box with periodic boundary conditions along all directions. Particle trajectories in the canonical ensemble are generated by following molecular dynamics (MD) at constant number–area–temperature (*NAT*). Temperature is measured in ε units with the Boltzmann constant, k_B = 1 and is maintained by a

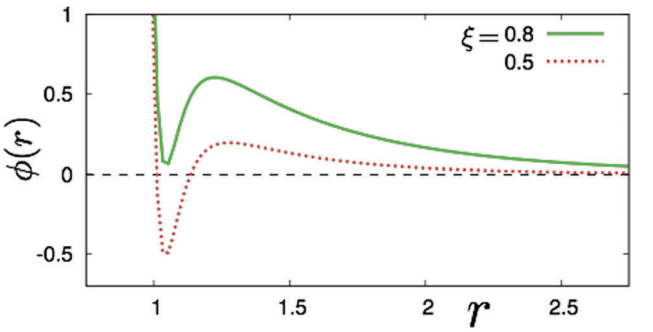

Fig. 1 The form of effective interaction $\phi(r)$ is shown for two different values of ξ = 0.5 and 0.8 setting A = 4.0 and α = 18. Note that the global attractive minimum becomes local with increasing ξ.

Langevin thermostat.[55] The motion of i-th particle with position vector $\mathbf{r}_i$ is expressed as follows,

$$\ddot{\mathbf{r}}_i = -\sum_{j\neq i} \nabla\phi(r) - \nu\dot{\mathbf{r}}_i + \zeta_i \qquad (3)$$

considering the force due to interaction $\phi(r)$ and frictional drag $\nu\dot{\mathbf{r}}_i$ from implicit media experienced by the particle. ζ_i is a random force with zero mean and Gaussian variance, $\langle\zeta_i(t_0)\zeta_j(t+t_0)\rangle = 2k_B(T/\nu)\delta_{i,j}\delta(t)$. Numerical integration is performed by using the velocity Verlet algorithm, as implemented in the LAMMPS simulation package,[56] with time steps $\delta t = 10^{-3}\tau$ where $\tau = \sigma/\sqrt{\varepsilon}$ a is for unit mass. The timescale of the simulation is set by τ and all temporal data presented later on are expressed in this unit. The system is first equilibrated at temperature $T_i = 1.0$ to form a simple liquid. The temperature of the equilibrated liquid is then linearly ramped down over 9.5×10^7 MD steps to final temperature $T_f = 0.05$ (see Fig. 2(a)). The temperature of the system thus drops by only $10^{-4}\varepsilon$ over unit time τ. For comparison, we note that the equilibrium liquid at $T_i = 1.0$ goes from the ballistic to diffusive regime in time slightly longer than τ. In other words, the system is allowed to lose only one unit of (kinetic) energy over a time period four orders of magnitude longer than the equilibrium diffusive time scale of the same. A slow cooling is chosen over the traditional fast quench to limit the influence of preparation rate dependence on the microscopic dynamics and focus on the effect of geometric frustration encoded by multiple length scales of the competing pair-wise interactions. Following the same cooling rate, systems at different final temperatures are also prepared by stopping the cooling at desired T_f starting from the same or statistically similar initial equilibrium configurations. We note that the system behaves as an equilibrium liquid over a range of final temperatures up to $T_f \sim 0.2$.

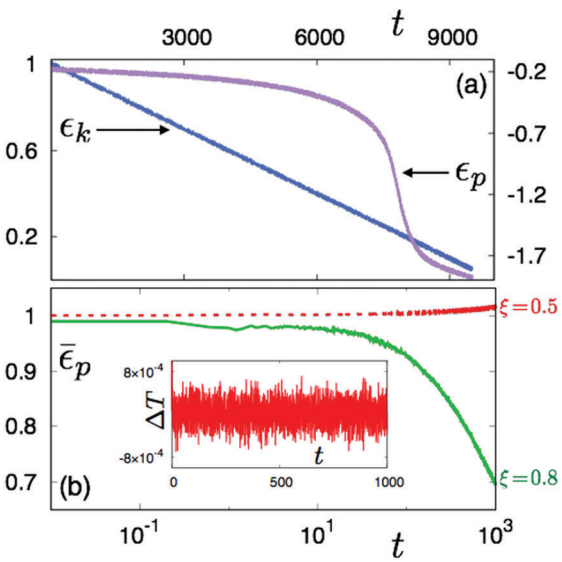

Fig. 2 (a) Linear cooling denoted by decreasing average instantaneous kinetic energy ε_k (blue) and corresponding variation of average potential energy ε_p (purple) are plotted for $\xi = 0.5$ and $\rho = 0.4$. Please note the sharp decrease in ε_p near $\varepsilon_k = 0.2$ which is close to the gas–liquid critical temperature for a system with bare attractive potential. Same linear cooling protocol is followed for other values of ξ reported and similar sharp drop in ε_p is observed around nearly same ε_k. (Inset) Shows the temporal evolution of temperature fluctuation (ΔT) over the 'observation period'. The fluctuation is measured by the difference between instantaneous kinetic energy and the mean kinetic energy over this time. (b) Time evolution of $\bar{\varepsilon}_p = \varepsilon_p(t)/\varepsilon_p(0)$ after the desired final temperature $T_f = 0.05$ is reached. (Inset) Shows the temperature fluctuation over this time. The systems, $\xi = 0.8$ (green) and $\xi = 0.5$ (red) are yet to reach equilibrium even after $10^3\tau$. Note that average ε_p changes sign from negative to positive as ξ is changed from 0.5 to 0.8.

Instantaneous temperature or kinetic energy per particle ε_k is shown in Fig. 2(a) during linear cooling. The potential energy per particle ε_p, following ε_k, shows an initial linear decay but drops abruptly around $T_f \sim 0.2$. We note that the gas–liquid critical temperature of the bare attractive potential ϕ_{SA} is $T_c = 0.18 \pm 0.01$.[57] This sharp drop of ε_p close to T_c is indicative of the effect of a phase separation process in the system. After reaching a desired final temperature, it is maintained by the same thermostat over a period of $10^3\tau$. This is our observation period when the trajectories are saved for further analysis. During this constant temperature observation time of three decades, ε_p continues to decay monotonically, which can be fitted well with a stretched exponential or a double-exponential function. To show this non-exponential time evolution of potential energy at constant temperature, we have plotted the scaled potential energy, $\bar{\varepsilon}_p = \varepsilon_p(t)/\varepsilon_p(0)$ for different ξ (see Fig. 2(b)). Please note that ε_p is negative for $\xi = 0.5$. It increases with increasing ξ and becomes positive for $\xi = 0.8$. Primary analysis of the temporal evolution of fluctuations in $\bar{\varepsilon}_p$ shows weak ergodicity breaking in absence of any external perturbation which should be credited to the geometric frustration originating from competing interactions. However, any conclusive remark in this regard requires further detailed study which is underway and will be reported elsewhere. In essence, the systems are yet to reach equilibrium even after this large waiting time. During this 'post cooling' period, the temperature fluctuations in the system remain very small and steady (see Fig. 2(b), inset). Most importantly, the size distribution of aggregates has reached its steady state, which is evident from the time-lapsed snapshots presented next in Fig. 3(a) and (b). Keeping these in mind, we expect that our observation time is sufficient to gather reliable statistics for both global and local dynamics of the system. Further, all the results presented next are averaged over 100 statistically independent initial conditions chosen from the equilibrium state of the respective systems.

Morphological variations from competing interactions

Aggregates may assume diverse morphologies ranging from finite-size non-compact to compact to percolated gel structures as a function of decreasing repulsion against attraction. In a previous study,[58] we have presented the structural hierarchy of the same model system for different realizations of competition controlled by α, A and ξ at a constant density and temperature. Percolated structures appearing at lower values of ξ (<0.5), are excluded from the present study. Here, we briefly describe two representative cases, $\xi = 0.5$ and 0.8, showing finite-size compact and non-compact aggregates, respectively. Note the

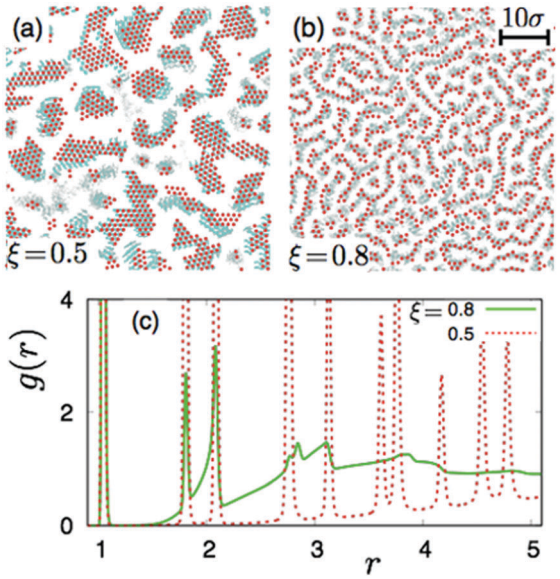

Fig. 3 Visual representation of particle dynamics for the two ξ values are shown for (a) compact (ξ = 0.5) and (b) non-compact (ξ = 0.8) structures, respectively, at final temperature T_f = 0.05 and ρ = 0.4. Only a part of the simulation box is shown for clarity. The scale used for both (a) and (b) is same and shown in (b). Each red filled circle denotes an instantaneous particle position. Blue background consists of dots representing the positions of the same particles for 100 earlier instants stored in a regular interval of 500 simulation steps. The size of the aggregates in both cases are clearly stable over this observation period of 5×10^4 steps or 50τ. (c) Radial distribution function $g(r)$ for these two values of ξ shows prominent split second peak indicating the formation of local structures. The difference in morphologies resulting from different values of ξ is also evident from the difference between corresponding $g(r)$.

dominant attraction well for ξ = 0.5 (Fig. 1), which is complemented by a small repulsive barrier slowly decaying at large r. The resulting configuration consists of perfect crystalline islands of exponentially distributed size. When ξ is raised to 0.8, the repulsive barrier increases significantly and the attractive minimum close to the particle core (r = 0) becomes comparable with the repulsive minimum far from the core (Fig. 1). Finite-size one-dimensional arrangements of particles are observed under such strong influence of repulsion. Upon further increase of ξ, the size of non-compact chain-like aggregates becomes smaller and the overall randomness in the configuration increases further.

A part of the 2D simulation box is presented in Fig. 3(a) and (b) showing both limiting morphologies, compact and non-compact, respectively. Red filled circles in these figures represent instantaneous particle positions. Positions of the same particles for 100 previous instants are plotted in the background with blue dots. All the collated configurations are separated from each other by 500 molecular dynamics steps. The slow dynamics experienced by the particles is already evident from these visual representations. Another important observation is the consistency of the collective dynamics of particles. Particles forming a cluster undergo collective translation and/or rotation; even bending to change conformations. However, fragmentation and reformation of aggregates are seldom observed. In other words, the system has reached its steady state at least in terms of the size of clusters.

The radial distribution function $g(r)$ for two limiting conformations, compact (ξ = 0.5) and non-compact (ξ = 0.8) is presented in Fig. 3(c). Also known as pair correlation function, $g(r)$ quantifies the probability of finding a particle from another arbitrary one as a function of the distance between them.

$$g(r) = (1/\rho)\langle\sum\delta(r - r_i)\rangle \quad (4)$$

Splitting of the second peak of $g(r)$ generally accounts for any local ordering in the system. In Fig. 3(c), we immediately notice the difference in the nature of splitting for the two different cases. The split second peak of $g(r)$ is asymmetric for ξ = 0.8 due to near linear branched conformation of aggregates, whereas it is symmetric and much pronounced for ξ = 0.5 as expected for compact crystalline arrangement of particles. In the next section, we unfold the microscopic dynamics across such morphologies obtained from the analysis of the simulated trajectories of constituent particles in terms of several measures of correlation.

3 Results

3.1 Local dynamics at fixed temperature

Non-Gaussian self displacement fluctuation. The statistics of individual displacement fluctuations for different local geometries for systems prepared at ρ = 0.4 at T_f = 0.05 is presented in this section. The probability of finding a normally diffusing particle is given by a Gaussian distribution with variance related to its long-time diffusivity. However, this distribution is often complemented by a fat exponential tail for systems exhibiting structural or dynamical heterogeneity.[59–61] We determine the probability of finding a particle at a distance $\mathbf{r}(t)$ from its arbitrarily chosen previous position $\mathbf{r}(0)$ by computing the self-part of van Hove function,[62]

$$G_s(r,t) = 1/N\sum_{i=1}^{n}\langle\delta(r - |\mathbf{r}_i(t) - \mathbf{r}_i(0)|)\rangle \quad (5)$$

Interestingly, a broad range of microscopic dynamics are captured by $G_s(r,t^*)$, with t^* = 50τ for aggregates across their morphological hierarchy. The choice of t^*, albeit arbitrary, is sufficiently large for the systems to settle in a steady state. For compact clusters, $G_s(r,t^*)$ is dominantly Gaussian with small exponential tail (Fig. 4(a)). On the contrary, for non-compact aggregates, Gaussian part of $G_s(r,t)$ is recessive and buried within the long exponential part (Fig. 4(b)). These two distinct parts immediately point to at least two different corresponding diffusivities[63] other than the average diffusivity and thus, the heterogeneous dynamics in the system. Example trajectories of a single particle chosen arbitrarily from the compact and non-compact clusters are drawn in Fig. 4(c) and (d) respectively with colours according to their time evolution. The spatial extent of the trajectory is restricted but jagged for compact aggregates compared to that of a non-compact one. From the visual inspection of these trajectories it is evident that in both cases, the particles undergo some sort of 'reside and jump' dynamics

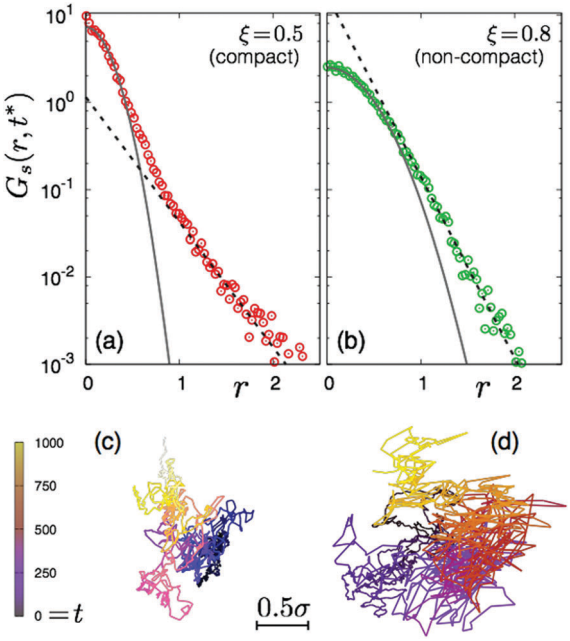

Fig. 4 Non-Gaussian behaviour of self-displacement fluctuations $G_s(r,t^*)$ (t^* = 50τ) is shown for (a) compact (ξ = 0.50) and (b) non-compact (ξ = 0.80) aggregates. Both systems have same ρ = 0.4 and T_f = 0.05. While dominant Gaussian self-fluctuations end with an exponential tail for compact clusters, displacement of a particle from its arbitrary origin is distributed exponentially over space for non-compact morphologies. (c) and (d) are trajectories of a single particle belonging to (a) and (b) respectively, colour coded by time. Using the same scale (scale bar = 0.5σ), it becomes evident that the particle trajectory (c) in compact clusters is more restricted and jagged than that in (d) non-compact clusters. The particle dynamics clearly changes accompanying the structural transition.

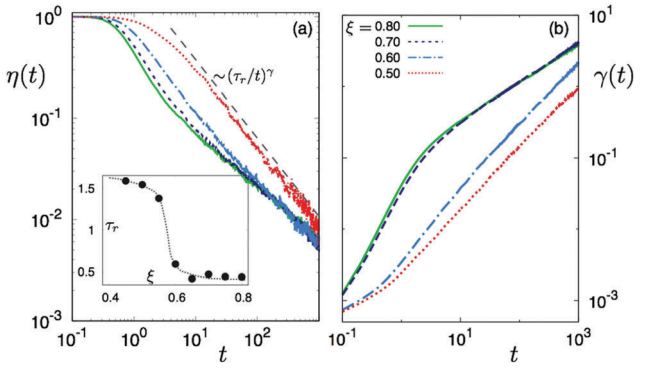

Fig. 5 At T_f = 0.05, (a) the self-overlap function $\eta(t)$ (see text) follows a power-law relation with time after an initial residence time τ_r. Across the morphological transition (compact to non-compact), the local dynamics shows a clear transition as τ_r jumps from high to low values (inset). This is one central result of the present study. (b) Temporal evolution of dynamic Lindemann parameter $\gamma(t)$ measuring the relative displacement fluctuation of particles with respect to its neighbours captures another aspect of this dynamical transition. Very slow initial increase in $\gamma(t)$ for compact aggregates clearly points to the caging of particles by their near-neighbours. On the other hand, initial steep increase followed by significant slowing down of $\gamma(t)$ at long-time can be attributed to binding in non-compact structures.

observed in other dynamically heterogeneous systems.[64] However, the associated time scales are expected to be different. We mention here that variations on non-Gaussian $G_s(r,t^*)$ have been reported in published literature but for unrelated systems such as granular materials close to jamming,[65] diffusing colloids on bio-filament network,[66] turbulence[67] and even for certain socio-economic setups.[68] By being able to capture this whole range of variations, our model system might be useful to understand the key ingredients of spatio-temporal heterogeneity arising under diverse situations.

Different time scales for different morphologies. We continue investigating average dynamics to study the overlap between two arbitrarily chosen instantaneous configurations in order to probe the degree of structural relaxation within the system. Quantification of the overlap[69,70] is computed as follows:

$$\eta(t) = \sum_{i,j=1}^{N} w\left(\left|\mathbf{r}_i(t) - \mathbf{r}_j(0)\right|\right) \quad (6)$$

where i, j are particle indices and $w(r)$ is a window function which is unity if $|\mathbf{r}_1 - \mathbf{r}_2| < a$ and zero otherwise. Allowing a particle to relax within certain threshold distance a from its original position, this quantity tells us whether a particle is knocked out by its own copy or any other particle at later time. We have chosen $a = 0.03\sigma$ as this is the average distance particles traverse in unit time τ. From the mean square displacement data (shown in the next section), we can easily identify this length scale. In Fig. 5(a), we show that configurations at T_f = 0.05 become uncorrelated in a scale-free manner from their arbitrarily chosen initial conformations after certain residence time τ_r. This feature is in contrast with the usual glassy systems where the relaxation of $\eta(t)$ is a stretched exponential[71] instead of being algebraic. The long-time algebraic tail of self-overlap can be explained in terms of a survival function of the form $(\tau_r/t)^\gamma$ where γ is the tail index[72] and τ_r is the minimum residence time of a particle. The typical τ_r is large for compact clusters ($\xi < 0.6$) and drops down at least by amount τ for non-compact conformations ($\xi > 0.6$). A clean step-like jump in τ_r, shown in Fig. 5(a)(inset), provides clear evidence of a change in fundamental time scales and thus the dynamics across the morphological hierarchy of aggregates. Note that this power-law behaviour for structural relaxation changes drastically to exponential decay when the final temperature of the system goes above T_f = 0.2 and behaves like an equilibrium liquid.

Symmetric caging *vs.* asymmetric binding. We identify different physical mechanisms responsible for the limiting cases of such heterogeneity using the evolution of relative displacement fluctuations. This is captured by calculating the dynamic Lindemann parameter,[73]

$$\gamma(t) = \langle[\Delta\mathbf{u}_j(t) - \Delta\mathbf{u}_{j+1}(t)]^2\rangle/2\sigma^2 \quad (7)$$

where $\Delta\mathbf{u}(t) = \mathbf{r}(t) - \mathbf{r}(0)$ is the displacement of a particle between its instantaneous position and its position at some arbitrarily chosen origin of time evolution prior to that instant. The indices j and $j + 1$ represent the neighboring particles within the first peak of the pair-correlation function $g(r)$. Expanding this equation can formally be rewritten as,

$$2\sigma^2\gamma(t) = \langle[\mathbf{u}_j(t) - \mathbf{u}_{j+1}(t)]^2\rangle + \langle[\mathbf{u}_j(0) - \mathbf{u}_{j+1}(0)]^2\rangle - 2\langle[\mathbf{u}_j(t) - \mathbf{u}_{j+1}(t)]\cdot[\mathbf{u}_j(0) - \mathbf{u}_{j+1}(0)]\rangle \quad (8)$$

Statistically, the last term should vanish if the motion of the particles are uncorrelated (as $t \to \infty$). This is indeed the case for an equilibrium liquid and $\gamma(t)$ should then go linearly with $\langle\Delta\mathbf{u}^2(t)\rangle$ where $\langle\cdots\rangle$ stands for the usual thermal averaging. Our computation, evidently, deviates from that in a systematic way. The particles in compact aggregates (ξ = 0.5, 0.6) show negligible or very little displacement with respect to their neighbors until time $\sim\tau$ (Fig. 5(b)). This observation combined with the previous 'reside and jump'-like dynamics hinted by $G_s(r,t)$ (Fig. 4) leads us to conclude the following. For compact clusters, caging of a particle occurs by its nearest neighbors arranged in a six-fold symmetry around it. Note that τ_r, presumably the residence time within the cage, is large for compact aggregates. After certain time, the particles leave the cage to move freely till they occupy another cage and $\gamma(t)$ increases monotonically with time. From visual inspection, we expect this to happen more frequently for the particles at the edge of a cluster and less frequently for those at the centre of compact crystalline aggregates. A reversal of this feature is observed for non-compact aggregates. Large repulsion responsible for these chain-like structures hinders the particles from being close to each other and $\gamma(t)$ shows a sharp initial increase. Consequently, τ_r is very small for such configurations as the particles, on an average, don't reside much longer at their original positions. However, once they are able to decrease their relative distance due to thermal fluctuations, side-wise binding of particles due to strong attraction leads to asymmetric structures and $\gamma(t)$ shows considerable decrease in the slope. In essence, as the aggregate morphology changes from compact to non-compact, the dynamics of constituent particles change from caging to asymmetric binding.

3.2 Global dynamics and temperature dependence

Intermediate relaxation and sub-diffusion. To analyse the global dynamics of constituent particles arranged in different local morphologies, we start with the mean square displacement of particles over the observation time. Mean square displacement (MSD) defined as,

$$\langle r^2(t)\rangle = \frac{1}{N}\sum_{i=1}^{N}\{r_i(t) - r_i(0)\}^2 \quad (9)$$

measures the spatial extent of a particle's displacement from its origin after which the particle diffuses randomly due to thermal fluctuations. In Fig. 6, we present the MSD data for different values of ξ for the final temperature T_f = 0.05 at fixed ρ = 0.4. One important observation is the presence of three distinct regimes of global dynamics. In addition to the usual two regimes, short-time ballistic and long-time diffusive, for equilibrium simple liquids, our model aggregate forming system shows a distinct intermediate time slow relaxation. Such behaviour is regarded as the signature of dynamical heterogeneity which is in line with our results for local dynamics presented in the previous section. The intermediate relaxation appears to be most strong for compact aggregates and gets softened with increasing ξ as the clusters become more non-compact. The system enters the long-time regime smoothly after this. The long-time dependence of MSD is generically expressed as $\langle r^2(t)\rangle \sim t^n$ where free diffusion is observed for n = 1. $n < 1$ indicates sub-diffusion[74] which is evident for all morphologies of aggregates and is also expected as

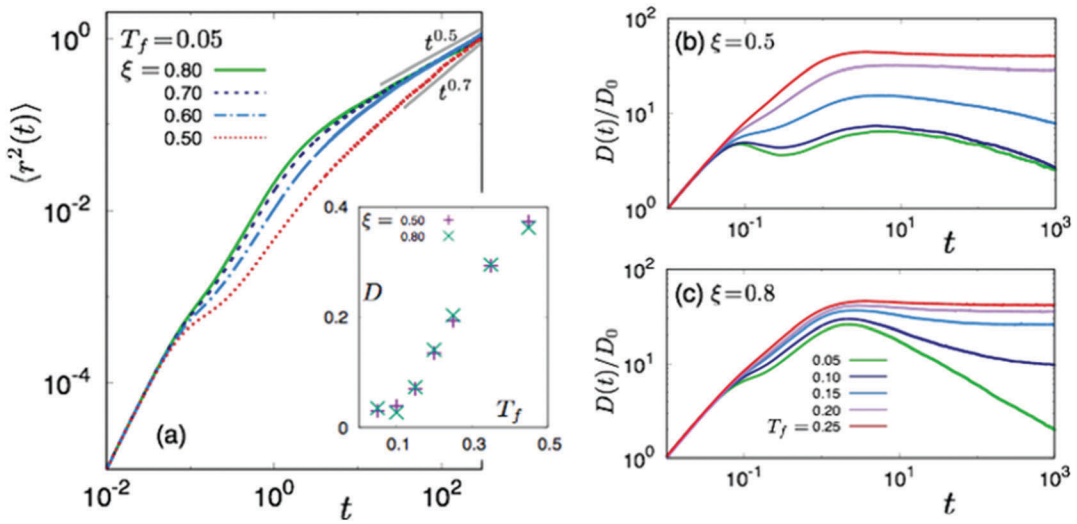

Fig. 6 (a) Mean square displacement (MSD) of particles is plotted against time for various values of ξ at fixed ρ = 0.4 and T_f = 0.05. MSD shows three distinct regimes, short-time ballistic, intermediate slow relaxation and long time sub-diffusive behaviour ($\langle r^2(t)\rangle \sim t^n$, $n < 1$). Intermediate slow relaxation is more prominent for compact clusters (ξ = 0.50) than the non-compact ones (ξ = 0.80). Although the exponent n varies with ξ, the diffusion constant D is insensitive to the structural variation. (Inset) Shows the dependence of diffusivity D on final temperatures T_f. Note that D, a measure of global dynamics of the system, is insensitive to local structure and primarily governed by temperature. Temperature dependence of time-dependent diffusion coefficient for (b) ξ = 0.50 (compact) and (c) ξ = 0.80 (non-compact). At the lowest final temperature, T_f = 0.05, the dynamics is heterogeneous but the time dependence varies with the morphology. The diffusion constant becomes time independent as temperature goes above T_f = 0.20 for both cases as both the systems become liquid and lose their structural signature.

we know our systems are yet to reach equilibrium within our observation time. The long-time diffusivity of the system, $D = \lim_{t\to\infty}(1/2dt)\langle r^2(t)\rangle$ is computed from the MSD data where d is the system's dimension. In Fig. 6 (inset), we show how D changes as a function of T_f for two distinct morphologies, compact (ξ = 0.5) and non-compact (ξ = 0.8). Surprisingly, D is very similar for both of these morphologies though the exponent n changes. These observations leads us to conclude that the global dynamics primarily maintained by the systems' temperature is an insufficient measure of spatio-temporal heterogeneity of aggregates.

Heterogeneous diffusion. Following our previous discussion on the average diffusivity D, here, we turn our attention to its temporal evolution. The time-dependent diffusion constant is defined as[75–77]

$$D(t) = \frac{\langle r^2(t)\rangle}{4t} \tag{10}$$

According to Fick's law, this quantity $D(t)$ should reach a steady state yielding a characteristic diffusion constant for a system in equilibrium. We note that spatial homogeneity is a primary assumption in such cases. As a corollary, we might expect $D(t)$ to be an indicator of heterogeneity and also its nature. In Fig. 6(a) and (b), we present $D(t)$ for two representative values ξ = 0.5 & 0.8, respectively, for a range of T_f. $D(t)$ is normalized by the short-time diffusivity $D_0 = \lim_{t\to 0} D(t)$ which represents particle motion in short-time ballistic motion when the particles have yet to experience the presence of their neighbours. In line with our observations of dynamical heterogeneity (previous section), $D(t)$ shows a monotonic decay at long time, $t > \tau$ for T_f = 0.05, the lowest temperature achieved in this study. Further, the decay process is clearly surrogate to the local morphology as $D(t)$ for compact structures (ξ = 0.5) is distinctly different from that of non-compact clusters (ξ = 0.8) at T_f = 0.05. As T_f increases beyond 0.2, the local structural ordering is destroyed and the system for all values of ξ behaves like equilibrium liquid as $D(t)$ becomes constant at long time. These results point to a fundamental relation between local finite-size morphology and global dynamics.

Diffusivity and structural randomness. Considering that diffusion in equilibrium simple liquids is governed by the Enskog process,[78] it is possible to relate the diffusivity of the system to the configurational phase space volume available to the same, quantified by the excess entropy of the system. The following phenomenological relation between diffusivity and excess entropy was proposed and established for simple equilibrium model systems.[79,80]

$$D = C\sigma^2\Gamma e^{S_2} \tag{11}$$

where C is a system dependent dimensionless non-zero constant and Γ is the typical collision frequency. The two-body excess entropy,[81] S_2, is an ensemble independent measure of structural randomness of the system.[82] It is computed from the static radial distribution function $g(r)$ of particles within a given system:

$$S_2 = -\rho/2\int \mathbf{dr}\{g(r)\ln g(r) - [g(r) - 1]\}. \tag{12}$$

Later, it was experimentally verified for colloidal systems[83] and a wide range of liquid metals.[84] In a previous study,[58] we categorized the morphological hierarchy of our model aggregates in terms of S_2. In short, non-compact clusters possess higher degree of randomness ($S_2 \sim 0$) closer to liquids. S_2 assumes large negative values as soon as local crystalline ordering appears within the system as in compact aggregates. Since for all these morphologies, the microscopic dynamics at low temperature is non-equilibrium and much slower than simple liquids, an Enskog process cannot be expected. Further, the collision frequency Γ is neither well defined nor readily accessible for the low temperature aggregates where the overall particle motion is very slow and collective. We define a dimensionless diffusivity $D^* = D/D_0$ and plot it against S_2 in Fig. 7 for different T_f. For $T_f \geq 0.2$, the fixed density system for all values of ξ studied shows the same D^* and S_2 as all of them behave like an equilibrium liquid. As the temperature goes lower, the system develops different structural randomness depending on its ξ value. A spread in both D^* and S_2 are now observed. Overall, an exponential relation, $D^* \sim e^{S_2}$ (similar to eqn (11)) is observed for systems with small values of $S_2(\leq 1)$ *i.e.* high-temperature equilibrium liquids and low-temperature, non-equilibrium non-compact aggregates. This observation is surprising and suggests that the Enskog process might not be limited to thermodynamic equilibrium, but instead is related to the morphological randomness. As the system adapts specific crystalline symmetry this feature breaks down and D^* becomes

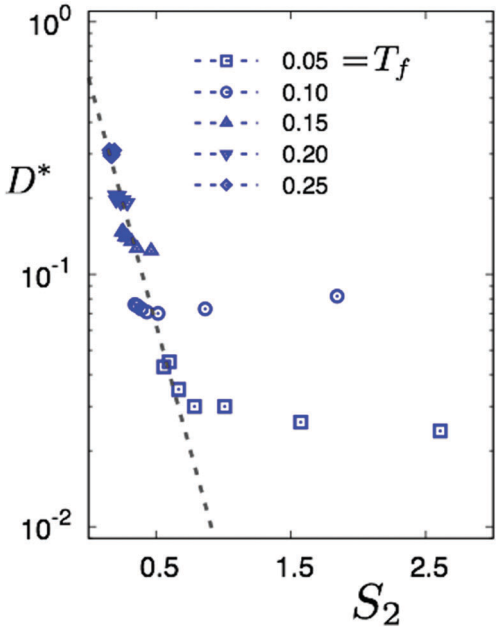

Fig. 7 The average dynamics of the system measured by reduced diffusivity D^* can be related to configurational randomness of the system measured by two-body excess entropy S_2. A universal D^*–S_2 relation (see text) is observed to hold for small values of S_2 or high randomness which correspond to high-temperature equilibrium liquid and low-temperature non-ergodic non-compact aggregates. The compact aggregates at low temperatures having local crystalline order naturally deviate from this universality.

nearly independent of S_2 for the compact aggregates as expected in equilibrium crystalline systems. With the possibility of a fundamental description of microscopic dynamics in terms of the degree of configurational randomness, this observation certainly begs further study.

4 Discussion

Inherent frustration of the competing short-range attraction and long-range repulsion results in restricted and random spatial extent of particle arrangements at low enough temperature and density. At the same time, the microscopic dynamics become heterogeneous as the mobility of particles becomes extremely sluggish due to the nominal thermal fluctuations. Importantly, both structural randomness of aggregates and heterogeneous micro-dynamics of constituent particles can be changed seamlessly by tuning the interactions under fixed thermodynamic conditions. Following the individual particle trajectories in different aggregate morphologies and the evolution of their fluctuations, we have identified the nature of these heterogeneous dynamics and its transition in sync with the morphological transition. However, we note that such differences are quiet subtle and are only revealed through comprehensive analysis. An average dynamical quantity such as the diffusion coefficient D of our model system is found to be insensitive to the observed structural hierarchy.

Under strong influence of short-range attraction, the movement of a particle is restricted within a cage bounded by its neighbors and particles align themselves in local hexagonal arrangement, energetically favored in 2D. Consequently, the self-displacement fluctuation $G_s(r,t)$ of particles forming a compact cluster is predominantly Gaussian within a length comparable to the typical cage size and decays exponentially outside this typical size due to the overall rearrangements happening within the system at that instant. With increasing repulsion, the degree of geometric frustration due to competition between interactions increases and the hexagonal symmetry becomes unfavorable. An emergent anisotropy originating from the complex interplay between enhanced frustration and thermal fluctuations allows only sidewise binding of particles. As a result, particles assume finite-size string-like non-compact structures and the Gaussian part of their $G_s(r,t)$ is almost hidden under the exponential part. These two distinct dynamical processes, caging and binding for compact and non-compact aggregates respectively, have further been supported by the detailed analysis of relative displacement fluctuation $\gamma(t)$ of particles relative to their nearest neighbors.

Following this physical picture, it is only natural to expect that the particles within a crystalline compact arrangement stay longer at and/or in close proximity to their original position compared to those in non-compact conformations. Investigation of the self-overlap function, $\eta(t)$, provides a useful description of such heterogeneous dynamics. Most importantly, this investigation identifies one fundamental measure of dynamics, namely, the residence time τ_r which clearly shows a transition in microscopic dynamics across different morphologies. Further correspondence between dynamics and morphology of aggregates has been established by relating scaled diffusivity and two-body excess entropy. Whereas these results might improve our current understanding[85] of the interrelation between structure and dynamics in condensed phases, the following questions are also invoked. Why and how exactly does the competing interaction affect the equilibration process of particulate systems? What is the distribution of diffusivity and how is it related to the vibrational modes of the system? Together with these questions, in future, we plan to investigate the effect of cooling rate, aging time and external mechanical fields on these pattern forming systems to understand the role of local geometry with unusual dynamical responses.

References

1 M. D. Ediger, *Annu. Rev. Phys. Chem.*, 2000, **51**, 99.
2 E. R. Weeks, J. C. Crocker, A. C. Levitt, A. Schofield and D. A. Weitz, *Science*, 2000, **287**, 627.
3 L. Berthier and G. Biroli, *Rev. Mod. Phys.*, 2011, **83**, 587.
4 P. J. Lu and D. Weitz, *Annu. Rev. Condens. Matter Phys.*, 2013, **4**, 217.
5 P. G. Wolynes, V. Lubchenko, *Structural Glasses and Supercooled Liquids: Theory, Experiment, and Applications*, John Wiley & Sons, 2012.
6 *Dynamical Heterogeneities in Glasses, Colloids, and Granular Media*, ed. L. Berthier, G. Biroli, J.-P. Bouchaud, L. Cipelletti and W. van Saarloos, Oxford University Press, 2011.
7 J. R. Bordin, A. B. de Oliveira, A. Diehl and M. C. Barbosa, *J. Chem. Phys.*, 2012, **137**, 084504.
8 L. B. Krott and M. C. Barbosa, *J. Chem. Phys.*, 2013, **138**, 084505.
9 D. Holcman and Z. Schuss, *J. Phys. A: Math. Theor.*, 2014, **47**, 173001.
10 Y. He, Y. Chen, H. Liu, A. E. Ribbe and C. Mao, *J. Am. Chem. Soc.*, 2005, **127**, 12202.
11 A. V. Tkachenko, *Phys. Rev. Lett.*, 2011, **106**, 255501.
12 F. Romano and F. Sciotino, *Soft Matter*, 2011, **7**, 5799.
13 Q. Chen, S. C. Bae and S. Granick, *Nature*, 2011, **469**, 381.
14 A. Jain, J. R. Errington and T. M. Truskett, *Soft Matter*, 2013, **9**, 3866.
15 W. M. Jacobs, A. Reinhardt and D. Frenkel, *Proc. Natl. Acad. Sci. U. S. A.*, 2015, **112**, 6313.
16 S. Whitelam, I. Tamblyn, J. P. Garrahan and P. H. Beton, *Phys. Rev. Lett.*, 2015, **114**, 115702.
17 P. C. Ohara, D. V. Leff, J. R. Heath and W. M. Gelbart, *Phys. Rev. Lett.*, 1995, **75**, 3466.
18 G. Markovich, D. V. Leff, S. W. Chung, H. M. Soyez, B. Dunn and J. R. Heath, *Appl. Phys. Lett.*, 1997, **70**, 3107.
19 D. L. Klein, R. Roth, A. K. L. Lim, A. P. Alivisatos and P. L. McEuen, *Nature*, 1997, **389**, 699.
20 J. R. Heath, P. J. Kuekes, G. Snider and R. S. Williams, *Science*, 1998, **280**, 1717.
21 W. A. Lopes and H. M. Jaeger, *Nature*, 2001, **414**, 735–738.
22 J. Groenewold and W. K. Kegel, *J. Phys. Chem. B*, 2001, **105**, 11702.

23 G. Malescio and G. Pellicane, *Nat. Mater.*, 2003, **2**, 97.
24 F. Sciortino, S. Mossa, E. Zaccarelli and P. Tartaglia, *Phys. Rev. Lett.*, 2004, **93**, 055701.
25 J. L. Lebowitz and O. Penrose, *J. Math. Phys.*, 1966, **7**, 98.
26 P. C. Hemmer and G. Stell, *Phys. Rev. Lett.*, 1970, **24**, 1284.
27 G. Stell and P. C. Hemmer, *J. Chem. Phys.*, 1972, **56**, 4274.
28 A. Stradner, H. Sedgwick, F. Cardinaux, W. C. K. Poon, S. U. Egelhaaf and P. Schurtenberger, *Nature*, 2004, **432**, 492.
29 T. H. Zhang, J. Klok, R. H. Tromp, J. Groenewolda and W. K. Kegel, *Soft Matter*, 2012, **8**, 667.
30 D. A. Weitz and M. Oliveria, *Phys. Rev. Lett.*, 1984, **52**, 1433.
31 D. A. Weitz, J. S. Huang, M. Y. Lin and J. Sung, *Phys. Rev. Lett.*, 1985, **54**, 1416.
32 E. Zaccarelli, G. Foffi, K. A. Dawson, S. V. Buldyrev, F. Sciortino and P. Tartaglia, *Phys. Rev. E: Stat., Nonlinear, Soft Matter Phys.*, 2002, **66**, 041402.
33 N. Gnan, G. Das, M. Sperl, F. Sciortino and E. Zaccarelli, *Phys. Rev. Lett.*, 2014, **113**, 258302.
34 G. Foffi, C. De Michele, F. Sciortino and P. Tartaglia, *Phys. Rev. Lett.*, 2005, **94**, 078301.
35 B. Ruzicka, E. Zaccarelli, L. Zulian, R. Angelini, M. Sztucki, A. Moussad, T. Narayanan and F. Sciortino, *Nat. Mater.*, 2011, **10**, 56.
36 E. Zaccarelli, P. J. Lu, F. Ciulla, D. A. Weitz and F. Sciortino, *J. Phys.: Condens. Matter*, 2008, **20**, 494242.
37 J. C. F. Toledano, F. Sciortino and E. Zaccarelli, *Soft Matter*, 2009, **5**, 2390.
38 F. Cardinaux, E. Zaccarelli, A. Stradner, S. Bucciarelli, B. Farago, S. U. Egelhaaf, F. Sciortino and P. Schurtenberger, *J. Phys. Chem. B*, 2011, **115**, 7227.
39 M. Carpineti and M. Giglio, *Phys. Rev. Lett.*, 1992, **68**, 3327.
40 M. Muschol and F. Rosenberger, *J. Chem. Phys.*, 1997, **107**, 1953.
41 P. Segre, V. Prasad, A. Schofield and D. Weitz, *Phys. Rev. Lett.*, 2001, **86**, 6042.
42 A. M. Kulkarni, N. M. Dixit and C. F. Zukoski, *Faraday Discuss.*, 2003, **123**, 3.
43 A. M. Puertas, M. Fuchs and M. E. Cates, *J. Chem. Phys.*, 2004, **121**, 2813.
44 J. L. Lebowitz, *Annu. Rev. Phys. Chem.*, 1968, **19**, 389.
45 P. J. Lu, E. Zaccarelli, F. Ciulla, A. B. Schofield, F. Sciortino and D. A. Weitz, *Nature*, 2008, **453**, 499.
46 R. P. Sear, *J. Chem. Phys.*, 1999, **111**(10), 4800.
47 A. Shukla, E. Mylonas, E. Di Cola, S. Finet, P. Timmins, T. Narayanan and D. I. Svergun, *Proc. Natl. Acad. Sci. U. S. A.*, 2008, **105**, 5075.
48 S. Srivastava, D. Nykypanchuk, M. Fukuto, J. D. Halverson, A. V. Tkachenko, K. G. Yager and O. Gang, *J. Am. Chem. Soc.*, 2014, **136**, 8323.
49 C. N. Likos, *Phys. Rep.*, 2001, **348**, 267.
50 G. A. Vliegenthart and H. N. W. Lekkerkerker, *J. Chem. Phys.*, 2000, **112**(12), 5364.
51 A. Puertas, C. De Michele, F. Sciortino, P. Tartaglia and E. Zaccarelli, *J. Chem. Phys.*, 2007, **127**, 144906.
52 T. Lafitte, S. K. Kumar and A. Z. Panagiotoloulos, *Soft Matter*, 2014, **10**, 786.
53 G. A. Vliegenthart, J. M. F. Lodge and H. N. W. Lekkerkerker, *Physica A*, 1999, **263**, 378.
54 J. L. Nugent, S. S. Moganty and L. A. Archer, *Adv. Mater.*, 2010, **22**, 3677.
55 T. Schneider and E. Stoll, *Phys. Rev. B: Condens. Matter Mater. Phys.*, 1978, **17**, 1302.
56 Available at http://lammps.sandia.gov.
57 P. Charbonneau and D. R. Reichman, *Phys. Rev. E: Stat., Nonlinear, Soft Matter Phys.*, 2007, **75**(5), 050401.
58 T. Das, T. Lookman and M. M. Bandi, *Soft Matter*, 2015, **11**, 6740.
59 E. R. Weeks, J. C. Crocker, A. C. Levitt, A. Schofield and D. Weitz, *Science*, 2000, **287**, 627.
60 W. K. Kegel and A. van Blaaderen, *Science*, 2000, **287**, 290.
61 P. Chaudhuri, L. Berthier and W. Kob, *Phys. Rev. Lett.*, 2007, **99**, 060604.
62 L. van Hove, *Phys. Rev.*, 1954, **95**, 249.
63 B. Wang, J. Kuo, S. C. Bae and S. Granick, *Nat. Mater.*, 2012, **11**, 483.
64 E. J. Saltzman and K. S. Schweizer, *Phys. Rev. E: Stat., Nonlinear, Soft Matter Phys.*, 2008, **77**, 051504.
65 J. Guan, B. Wang and S. Granick, *ACS Nano*, 2014, **8**, 3331.
66 K. C. Leptos, J. S. Guasto, J. P. Gollub, A. I. Pesci and R. E. Goldstein, *Phys. Rev. Lett.*, 2009, **103**, 198103.
67 B. I. Shraiman and E. D. Siggia, *Nature*, 2000, **405**, 639.
68 S. R. Majumder, D. Diermeier, T. A. Rietz and L. A. N. Amaral, *Proc. Natl. Acad. Sci. U. S. A.*, 2009, **106**, 679.
69 G. Parisi, *J. Phys. A: Math. Gen.*, 1997, **30**, L765.
70 S. C. Glotzer, V. N. Novikov and T. B. Schrøder, *J. Chem. Phys.*, 2000, **112**, 509.
71 S. Karmakar, C. Dasgupta and S. Sastry, *Proc. Natl. Acad. Sci. U. S. A.*, 2009, **106**, 3675.
72 M. E. J. Newman, *Contemp. Phys.*, 2005, **46**, 323–351.
73 K. Zahn, R. Lenke and G. Maret, *Phys. Rev. Lett.*, 1999, **82**, 2721.
74 S. Havlin and D. Ben-Avraham, *Adv. Phys.*, 2002, **51**, 187.
75 M. J. Saxton, *Biophys. J.*, 1994, **66**, 394.
76 M. J. Saxton, *Biophys. J.*, 1996, **70**, 1250.
77 M. J. Saxton, *Biophys. J.*, 1997, **72**, 1744.
78 S. Chapman and T. G. Cowling, *The Mathematical Theory of Non-Uniform Gases*, Cambridge University Press, London, 1970.
79 Y. Rosenfeld, *Phys. Rev. A: At., Mol., Opt. Phys.*, 1977, **15**, 2545–2549.
80 M. Dzugutov, *Nature*, 1996, **381**, 137.
81 R. E. Nettleton and M. S. Green, *J. Chem. Phys.*, 1958, **29**, 1365.
82 A. Baranyai and D. J. Evans, *Phys. Rev. A: At., Mol., Opt. Phys.*, 1989, **40**, 3817.
83 X. Ma, W. Chen, Z. Wang, Y. Peng, Y. Han and P. Tong, *Phys. Rev. Lett.*, 2013, **110**, 078302.
84 J. Hoyt, M. Asta and B. Sadigh, *Phys. Rev. Lett.*, 2000, **85**, 594–597.
85 I. M. Sokolov, *Soft Matter*, 2012, **8**, 9043.